

Superconductor Science and Technology

PAPER • OPEN ACCESS

Anisotropy of flux pinning properties in superconducting (Li,Fe)OHFeSe thin films

To cite this article: Jens Hänisch *et al* 2020 *Supercond. Sci. Technol.* **33** 114009

View the [article online](#) for updates and enhancements.


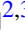






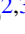


IOP | ebooks™

Bringing together innovative digital publishing with leading authors from the global scientific community.

Start exploring the collection—download the first chapter of every title for free.

Anisotropy of flux pinning properties in superconducting (Li,Fe)OHFeSe thin films

Jens Hänisch¹ , Yulong Huang^{2,3,7} , Dong Li^{2,3} , Jie Yuan^{2,4} , Kui Jin^{2,3,4} , Xiaoli Dong^{2,3,4} , Evgeny Talantsev^{5,6} , Bernhard Holzapfel¹  and Zhongxian Zhao^{2,3,4} 

¹ Karlsruhe Institute of Technology, Institute for Technical Physics, Hermann-von-Helmholtz-Platz 1, 76344, Eggenstein-Leopoldshafen, Germany

² Beijing National Laboratory for Condensed Matter Physics and Institute of Physics, Chinese Academy of Science, People's Republic of China

³ University of Chinese Academy of Sciences, Beijing, People's Republic of China

⁴ Songshan Lake Materials Laboratory, Dongguan, Guangdong 523808 People's Republic of China

⁵ M.N. Mikheev Institute of Metal Physics, Ural Branch, Russian Academy of Sciences, 18 S Kovalevskoy St, Ekaterinburg 620108 Russia

⁶ Nanotech Centre, Ural Federal University, 19 Mira St., Ekaterinburg 620002 Russia

E-mail: jens.haenisch@kit.edu

Received 23 February 2020, revised 30 June 2020

Accepted for publication 20 August 2020

Published 19 October 2020



CrossMark

Abstract

The electrical transport properties of (Li,Fe)OHFeSe films have been investigated in detail. The sharply textured films, prepared by matrix-assisted hydrothermal epitaxy (MHE) on LaAlO₃, show a zero-resistance critical temperature T_c of ~ 42 K, J_c values well above 1 MA cm^{-2} at low temperatures, and a maximum pinning force density F_p of $\sim 100 \text{ GN m}^{-3}$ at 4 K. The activation energy U_0 for thermal depinning of flux lines has been resolved for low magnetic fields, it agrees well with literature data. The coherence lengths and penetration depth were estimated via upper critical field B_{c2} and self-field J_c , respectively, to be $\xi_{ab} \sim 2.7 \text{ nm}$, $\xi_c = 0.24 \text{ nm}$, and $\lambda_{ab} \sim 160\text{--}200 \text{ nm}$. The layered crystal structure leads to highly anisotropic and two-dimensional electrical properties, including trapping and lock-in of vortices.

Keywords: Fe-based superconductors, (Li, Fe)OHFeSe, pinning, activation energy, anisotropy, thin films

(Some figures may appear in colour only in the online journal)

1. Introduction

In the last 10 years, investigations on Fe-based superconducting (FBS) thin films have concentrated mainly

on three crystal classes [1, 2]: the FeSe-based structures (mostly FeSe_{1-x}Te_x), BaFe₂As₂- and SrFe₂As₂-based structures (mostly Ba(Fe,Co)₂As₂), and LnFeAsO-based structures (Ln lanthanide, mostly NdFeAs(O,F) and SmFeAs(O,F)), often abbreviated for their main stoichiometry, *11*, *122*, and *1111*. The main deposition techniques are pulsed laser deposition (PLD) for *11* and *122*, and molecular beam epitaxy (MBE) for *1111* and compounds with volatile elements, such as K and Ca. Besides those highly investigated structures, a single study on LiFeAs grown by MBE has been reported [3]. Recently, a fifth FBS crystal structure has been successfully deposited as thin film: (Li,Fe)OHFeSe (*11111*)

⁷ Now at University of Buffalo, USA.



Original content from this work may be used under the terms of the [Creative Commons Attribution 4.0 licence](https://creativecommons.org/licenses/by/4.0/). Any further distribution of this work must maintain attribution to the author(s) and the title of the work, journal citation and DOI.

by matrix-assisted hydrothermal epitaxy (MHE) process in a soft-chemical method [4], which enabled electrical transport measurements with high voltage resolution and especially transport J_c measurements on this compound. This crystal structure, discovered in 2014 by Lu *et al* [5] and shortly after investigated by Pachmeyer *et al* [6,], Sun *et al* [7], and Dong *et al* [8, 9], can be regarded in two ways: On the one hand it resembles the 1111 crystal structure if the hydroxyl group is regarded as single entity. It therefore may be seen as the chalcogenide equivalent of the pnictide 1111 compounds. On the other hand, one may think of the structure as FeSe with large spacer layer (Li,Fe)OH, i.e. expanded c -axis lattice parameter. It is therefore a link between bulk samples of the most simple FBS structure FeSe, e.g. [10, 11], with critical temperatures $T_c \sim 10$ K and single-unit-cell films of FeSe on SrTiO₃ with a superconducting gap opening above 65 K [12]. With the latter, (Li,Fe)OHFeSe shares a similar electronic structure consisting of electron pockets near the Brillouin zone corners, as observed by angle-resolved photo emission spectroscopy (ARPES) [13], and therefore similar electronic properties, namely highly 2D, electron-dominated multi-band superconductivity with strong 2D spin fluctuations [9].

These 1111 films grow epitaxially with a very sharp c -axis orientation, have the expected T_c of ~ 42 K for optimal carrier doping and showed high critical current densities J_c of 0.5 MA cm^{-2} at 24 K ($t = T/T_c = 0.57$) [14]. Until now, details of the flux pinning behaviour and especially the field orientation dependence of J_c are missing for these films. Here, we report on such measurements and compare the results to pnictide 1111 films as well as cuprate superconductors where appropriate.

2. Sample preparation and experimental details

The films are prepared by MHE, a soft-chemical method as described in [4] and [14]. In summary, large insulating $\text{K}_{0.8}\text{Fe}_{1.6}\text{Se}_2$ single crystals attached to LaAlO_3 serve as matrix for the crystalline film to grow in between. The structural quality of the films was determined by x-ray diffraction (XRD) with $\text{Cu K}\alpha_1$ radiation ($\lambda = 1.5405 \text{ \AA}$) on a Rigaku SmartLab equipped with two $\text{Ge}(220)$ monochromators. The superconductivity and critical temperature were characterized both via the diamagnetization transition on a Quantum Design MPMS-XL1 system and via the resistive transition in $R(T)$. Two films of the same batch (sample B) were patterned mechanically into microbridges of 50 and 20 μm width respectively and ~ 0.5 mm length, at which the electrical transport properties were measured in 4-point geometry and maximum Lorentz force configuration in a Quantum Design PPMS in magnetic fields up to 14 T. A sample of a different batch (sample A) with similar properties was used for the J_c data for $B_{\parallel c}$. The thickness of the films was estimated to be ~ 150 nm and ~ 200 nm respectively. J_c was determined with an electric field criterion of $1 \mu\text{V cm}^{-1}$ from $V(I)$ curves. The resistance R was measured with constant current of 10 mA, irreversibility field B_{irr} and T_{c0} were determined with a criterion of $R = 1 \text{ m}\Omega$ and the upper critical field B_{c2} at $R = 8 \Omega = 50\% R_n$, where R_n is

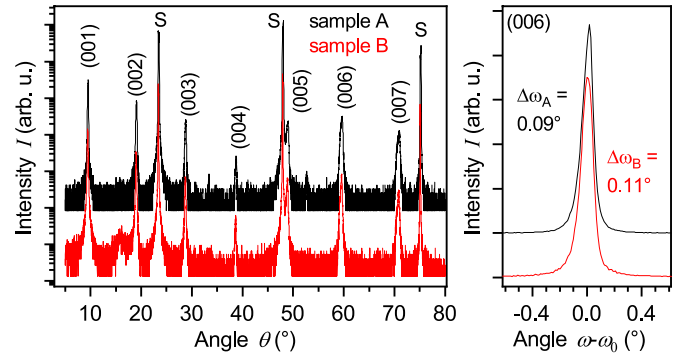


Figure 1. X-ray diffraction ($\text{Cu K}\alpha_1$ ($\lambda = 1.5405 \text{ \AA}$)) of investigated (Li,Fe)OHFeSe films. Left θ - 2θ scans in logarithmic presentation, right (006) rocking curves. S: substrate peaks of LaAlO_3 .

the normal state resistance just above T_c . A 50% criterion was chosen instead of the usual 90% in order not to probe the large fluctuation region, which is due to the large crystallographic and electronic anisotropy.

The samples of this study show very clean θ - 2θ scans with only (00 l) reflections indicating highly oriented c -axis growth, figure 1. The (006) rocking curves have a full width at half maximum of 0.09° (sample A) and 0.11° (sample B). The c -axis parameters, calculated by the Nelson-Riley method [15] are $0.9302(2) \text{ nm}$ and $0.93004(4) \text{ nm}$ respectively, which in combination with the T_c values (see figure 2(c) in [4]) means the samples are optimally doped and far away from the region of antiferromagnetic (afm) ordering [16].

3. Resistive transition and activation energy U_0

The resistive transition in several magnetic fields $B = \mu_0 H$, as shown in figure 2, shows strong broadening for increasing $B_{\parallel c}$ [a field as low as 15 mT leads to a T_{c0} shift of 1 K, inset figure 2(a)] and strong anisotropy between the two main directions $B_{\parallel c}$ and $B_{\parallel ab}$, similar to the observations in reference [14]. The T_{c0} value 42.0 K agrees well with the onset temperatures of the magnetization curves.

While the temperature dependence of the upper critical field $B_{c2}(T)$ for $B_{\parallel c}$ shows a positive curvature near T_c (possibly due to multiband effects), both $B_{c2}(T)$ curves are rather linear above ~ 2 T. The slopes $S' = |dB_{c2}/dT|$ above 3 T are 1.5 T K^{-1} and 16.5 T K^{-1} for $B_{\parallel c}$ and $B_{\parallel ab}$ respectively. With the WHH formula $B_{c2}^{\text{orb}}(0) = 0.69 S' T_c$ [17], this translates to orbital $B_{c2}(0)$ values of 44 T and 485 T as well as in-plane coherence length of $\xi_{ab} = 2.7 \text{ nm}$ and out-of-plane coherence length $\xi_c = 0.24 \text{ nm}$ and an electronic mass anisotropy $\gamma = \xi_{ab}/\xi_c = 11$ near T_c . The corresponding data for sample A and $B_{\parallel c}$ are $S'_c = 1.65 \text{ T K}^{-1}$, $B_{c2}^c(0) = 49 \text{ T}$ and $\xi_{ab} = 2.6 \text{ nm}$. These ξ_{ab} values are in good agreement with values obtained in a simple WHH two-band model according to [18, 19] on the full data set 0 T–14 T, whereas such two-band fits in the Gor'kov [20] and Jones, Hulm, and Chandrasekhar (JHC) [21] approximation result in slightly higher respectively lower values. Caution should be paid nevertheless, since the calculated $B_{c2}^{\text{orb}}(0)$ and hence ξ values are criterion- and

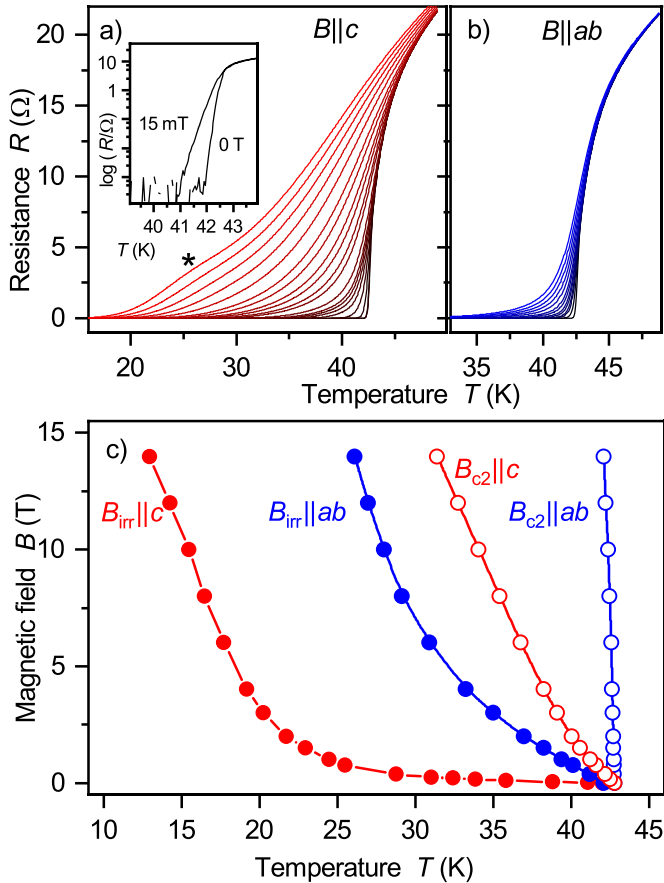


Figure 2. Resistive transition for $B||c$ (a) and $B||ab$ (b) and according phase diagram of a (Li,Fe)OHFeSe film (c). Applied fields were 0, 375, 500, 750 mT, 1, 1.5, 2, 3, 4, 6, 8, 10, 12, 14 T for both directions and additionally 15, 50, 100, 150, 200, 250 mT for $B||c$. Criteria were $R = 1 \text{ m}\Omega$ (noise level) for B_{irr} and $R = 8 \Omega = 50\% R_n$ for B_{c2} . * shoulder feature, for explanation see text.

method-dependent, as illustrated in ref [22] for FeSe single crystals. The anisotropy of ~ 11 is in good agreement with the penetration depth anisotropy of ~ 10 from muon spin resonance (μSR) measurements [23] and with the ξ anisotropy from resistive measurements [24] but larger than other literature data of ~ 4 [9] and ~ 7 [25, 26]. Interestingly, no correlation between T_c and γ was found.

There is a slight shoulder at ~ 25 K observed for the highest fields $B||c$ (marked with a star in figure 2(a)), which can also be seen in refs. [14]. This is most likely a phase transition in the vortex liquid region, i.e. the vortex decoupling transition between 3D and 2D liquid as also seen for strongly anisotropic cuprate superconductors, such as $\text{Bi}_2\text{Sr}_2\text{CaCu}_2\text{O}_{8-\delta}$ [27]. For completeness, this behaviour is also sometimes observed for polycrystalline samples, e.g. for a LaFeAs(O,F) film (figure 2 in [28]). Such a grain boundary scenario can be excluded here due to the high phase purity and degree of texture of the samples.

The activation energy U_0 of our film, figure 3, as estimated from linear fits of $R(T)$ near B_{irr} in Arrhenius representation is very similar to literature data on single crystal

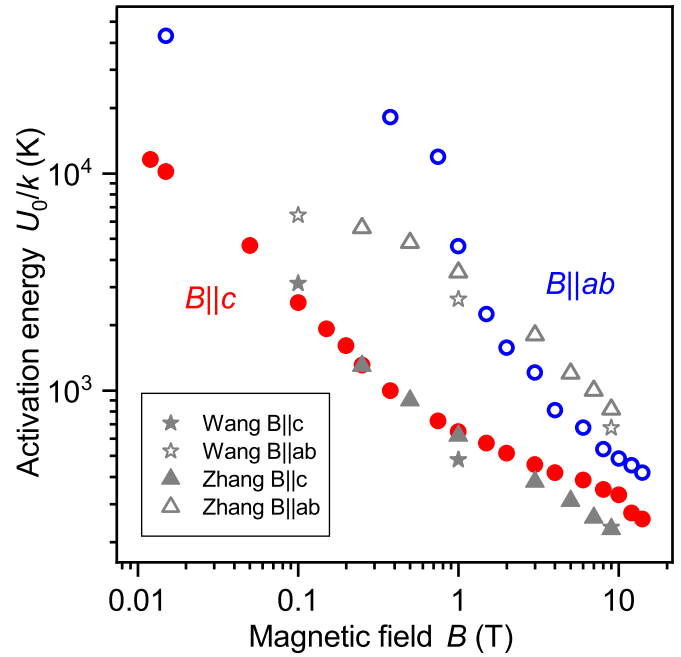


Figure 3. Field dependence of the activation energy U_0 of a (Li,Fe)OHFeSe film for $B||c$ and $B||ab$ in comparison to literature data on single crystal samples by Wang *et al* [24] and Zhang *et al* [26].

samples [24, 26], except for low fields $B||ab$. For this field and orientation range, the error bars are considerable due to low number of data points, which often leads to an underestimation of U_0 . The activation energy also shows strong anisotropy, especially at low fields. A characteristic kink for $B||c$ and strong reduction for $B||ab$ at ~ 0.7 T indicates an anisotropic change in pinning mechanism with a second regime of single vortex pinning at medium fields for $B||c$. As can be seen in table 1, U_0 is strongly influenced by T_c and the electronic anisotropy (or degree of two-dimensionality). FeSe and Fe(Se,Te) with lower T_c and lower anisotropy show similar values, FeSe unit-cell films on SrTiO_3 [29, 30] (2D and high T_c) show lower U_0 values than (Li,Fe)OHFeSe, and pnictide NdFeAs(O,F) films [31, 32] with similar crystal structure and T_c but lower anisotropy than (Li,Fe)OHFeSe show roughly 4 times larger values.

4. Critical current densities

4.1. Temperature and field dependence of J_c for $B||c$

J_c in (Li,Fe)OHFeSe films is highly temperature-and-field dependent, figures 4 and 5. Due to the very low irreversibility line at temperatures above ~ 25 K, figure 2(c), J_c decreases by one order of magnitude from self-field to an applied field of 200 mT, figure 4. In the temperature range around 15–20 K, where $B_{\text{irr}}^||c$ starts to rise considerably, J_c is only weakly field-dependent in the low-to-medium field range (0.2–1 T). Here, $J_c(T)$ shows a slight positive curvature for small applied fields which indicates the inset of a possible different pinning mechanism, which has to be investigated in

Table 1. Thermal activation energy U_0 at 1 T for $B||c$ for several FeSe-based compounds [FeSe, Fe(Se,Te), (Li,Fe)OHFeSe] as well as $Ln1111$ compounds ($Ln = La, Nd, Sm$). T_c values (determined as onset T_c , $T_c^{90\%}$ or in case of (Li,Fe)OHFeSe $T_c^{50\%}$) as well as the anisotropy parameter γ (determined from the ratio of the $B_{c2}(T)$ slopes near T_c) are given as well.

Compound	$U_0/k(1 \text{ T} c)$ (K)	γ	T_c (K)	Ref.
FeSe film	800	2.3	11.0	[33]
FeSe _{0.6} Te _{0.4} film	5500	3.8	21.0	[34]
FeSe _{0.45} Te _{0.55} sc	850	-	14.4	[35]
FeSe _{0.4} Te _{0.6} sc	340	1.45	14.2	[36]
(Li,Fe)OHFeSe sc	480	12.5	35.4	[24]
(Li,Fe)OHFeSe sc	600	7.6	37.2	[26]
(Li,Fe)OHFeSe film	650	11	42.5	This work
FeSe 1uc	240	2D	38	[29]
FeSe 1uc	21	2D	27	[30]
LaFeAs(O,F) film	220	4.8	23	[31, 32]
NdFeAs(O,F) film	2700	~4.5	44	[32]
SmFeAs(O,F) film	7300	5.5	53.5	[37]

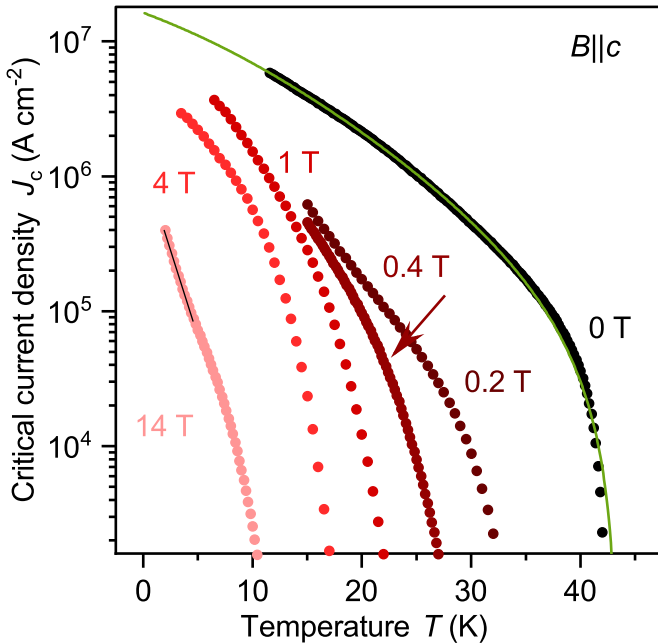


Figure 4. Temperature dependence of J_c for several applied magnetic fields $B||c$. The green line is a fit according to equations (6)–(11) of [39]. Within the p -wave assumption as an example. The extrapolated $J_c^{\text{sf}}(T)$ is 16 MA cm^{-2} . Black line: fit of equation (2) for weak pinning at 14 T.

more detail in a future study. Below that temperature, the data for medium fields (1 T, 4 T) are well described by strong pinning [38]:

$$J_c^{\text{str}}(T) \sim \exp \left\{ -3 \left(\frac{T}{T^*} \right)^2 \right\} \quad (1)$$

while for the high-field data at 14 T an additional weak-pinning contribution [40]:

$$J_c^{\text{wk}}(T) \sim \exp \left\{ -\frac{T}{T_0} \right\} \quad (2)$$

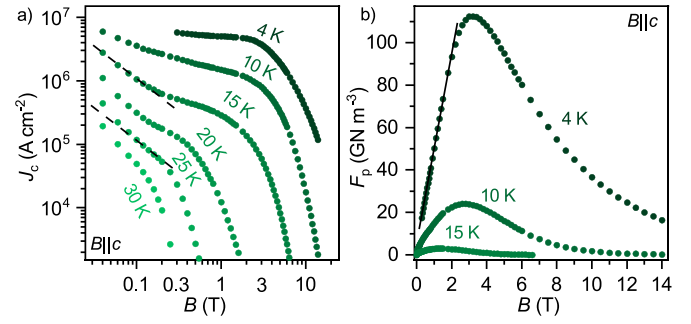


Figure 5. Magnetic field dependence of J_c (a) and corresponding F_p (b) of a (Li,Fe)OHFeSe film for several temperatures. Dotted line: $J_c \sim B^{-1}$, full line $F_p \sim B$.

at low temperatures is visible which can be ascribed to disorder at the atomic scale. Whether such a contribution is present at lower fields could not be determined due to limitations in cooling power. $k_B T^*$ and $k_B T_0$ are the characteristic energy scales for both types of pinning which have characteristic temperatures of $T^* = 23, 19,$ and 13 K for 1 T, 4 T, and 14 T respectively, and $T_0 = 4 \text{ K}$ for 14 T. These values are much lower than for YBCO coated conductors [41], which is again explained by lower T_c and higher anisotropy values.

Disregarding a very slowly varying pre-factor of $[\ln(\lambda/\xi) + 0.5]$, the self-field critical current density $J_c^{\text{sf}}(T)$ of thin films whose thickness is much smaller than the London penetration depth in c -direction, $2b \ll \lambda_c(0)$, is practically solely determined by the in-plane superfluid density, $\rho_{s,ab}(T)$, to the power of 1.5, $\rho_s^{1.5}(T) = \frac{1}{\lambda^3(T)}$, and hence by the penetration depth $\lambda_{ab}(T)$ [42]:

$$J_c^{\text{sf}}(T) = \frac{B_{c1,c}(T)}{\mu_0 \lambda_{ab}(T)} = \frac{\Phi_0}{4\pi\mu_0} \cdot \frac{\ln \left(\frac{\lambda_{ab}(T)}{\xi_{ab}(T)} \right) + 0.5}{\lambda_{ab}^3(T)} \quad (3)$$

where Φ_0 is the magnetic flux quantum, μ_0 the magnetic permeability of free space, and $B_{c1}(T)$ the lower critical field.

The $J_c^{\text{sf}}(T)$ data have been fitted with regard to a possible p -wave symmetry in Fe-based superconductors according to equations 6–11 in [39], green line in figure 4. Input parameters were the geometrical dimensions of the sample and the anisotropy $\gamma = 11$. The best fit was achieved with deduced parameters of $T_c = 43.4 \text{ K}$, the BCS ratio for energy gap to the transition temperature of $2\Delta(0)/kT_c = 3.24$, and $\lambda_{ab}(0) = 160 \text{ nm}$ corresponding to extrapolated $J_c^{\text{sf}}(T \rightarrow 0) \sim 16 \text{ MA cm}^{-2}$. This fit is one possibility and the extrapolated $\lambda_{ab}(0)$ value a lower limit, since fittings to other symmetries (i.e. s - and d -wave) yield equally good fits for the available data range and slightly larger $\lambda_{ab}(0)$ values (up to 200 nm). Two-band fits (as shown for μSR data in [23]) were not reasonably possible due to the lack of low- T $J_c^{\text{sf}}(T)$ data. Nevertheless, the extrapolated $\lambda_{ab}(0)$ is considerably lower than evaluated in literature (e.g. 280 nm [23] or 360 nm [39]). Since the relative errors relate as $\Delta\lambda/\lambda = 1/3 \Delta J_c/J_c$, these literature values are outside the expected range of $\lambda_{ab}(0)$ for a

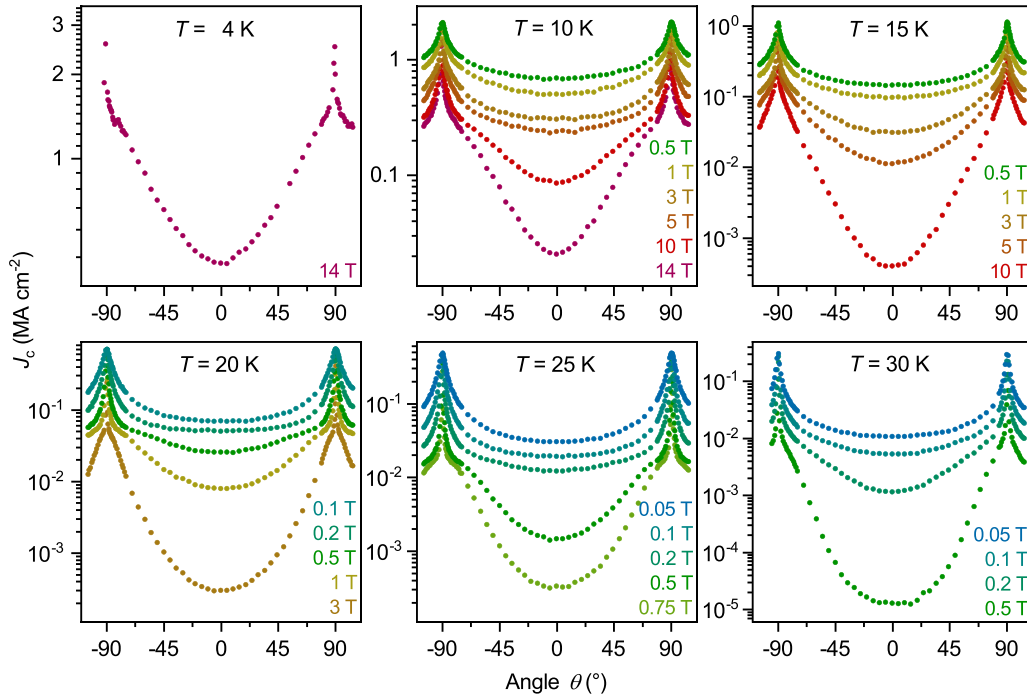


Figure 6. Angle dependence of the critical current density J_c for several fields and temperatures where the angle θ is defined between applied magnetic field B and crystallographic c -axis.

reasonable uppermost estimate of $\Delta J_c/J_c \sim 30\%$. Ground-state λ values of nominally the same compound commonly vary strongly between measurement runs and groups (see for instance the literature values for the cuprate $\text{Sr}_{0.9}\text{La}_{0.1}\text{CuO}_2$ ranging from 93.2 nm [43] via 116 nm [44] to 272 nm [45] for samples of the same optimal $T_c \sim 43$ K) and depend on the measurement technique (with μSR usually yielding somewhat larger values). Nevertheless, the result of a smaller penetration depth in this film sample compared to crystalline bulk is reasonable, since the film has a higher T_c , which to first approximation corresponds to a larger superfluid density. A value of $\lambda_{\text{ab}}(0) \sim 200$ nm has also been assumed by Yi *et al* [46].

The Ginzburg-Levanyuk number, which is a measure for the range of fluctuations, is given by [47]:

$$Gi = 1.07 \cdot 10^{-13} \frac{\kappa_c^4 T_c^2 \gamma^2}{\mu_0 H_{c2}} \quad (4)$$

which yields with the same estimates of the material parameters $Gi = 6.7\text{--}18.3 \times 10^{-3}$, comparable to $\text{FeSe}_{0.5}\text{Te}_{0.5}$ ($Gi = 17.23 \times 10^{-3}$) and $\text{NdFeAs}(\text{O},\text{F})$ ($Gi = 6.53 \times 10^{-3}$) [47].

Returning to the in-field performance of the sample, it is noticeable that the field dependence of J_c varies strongly with temperature and field range, figure 5(a). J_c decreases roughly as $J_c \sim B^{-1}$ with applied field at high temperatures and low fields (dashed lines, figure 5(a)), which indicates strong pinning at small ($\sim \xi$) random pinning centres [48]. In contrast, J_c is rather constant at 4 K and medium fields of 1–2 T, which manifests itself in a linear dependence of the pinning force density with field in this region, black line in figure 5(b).

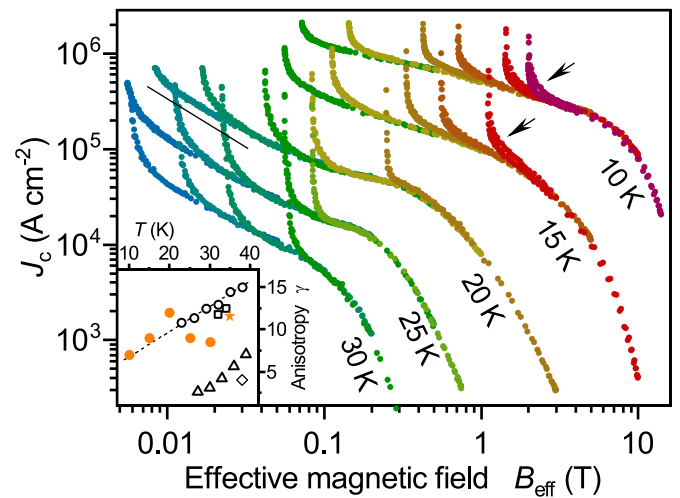


Figure 7. Scaling of $J_c(\theta)$ data of figure 5 within the single-band anisotropic Ginzburg-Landau approach. Arrows: asymmetries of $J_c(\theta)$, black line: $J_c \sim B_{\text{eff}}^{-1}$. Inset: Temperature dependence of the scaling parameter γ and comparison to B_{c2} anisotropies in literature (\diamond [9], \square [24], \triangle [25], \circ [46]), \star B_{c2} anisotropy determined by the slopes $dB_{c2}/dT|_{T_c}$ in the range 3–14 T.

Here, the pinning force density per unit length of an individual flux line can be estimated as $f_p' = \frac{\partial F_p}{\partial B} \Phi_0 \sim 10^{-4} \text{ N m}^{-1}$. The maximum achievable pinning force per length for strong pinning is $f_p' = 0.45 \pi \xi \mu_0 H_c^2 \sim 1.4 \cdot 10^4 \frac{\Phi_0^2}{\xi_{\text{ab}} \lambda_{\text{ab}}^2}$ [49] (eq. 6.7) which yields $5.5\text{--}8.7 \cdot 10^{-4} \text{ N m}^{-1}$ for the values of $\xi(0)$ and $\lambda(0)$ given above. That means, taking into account an uncertainty of

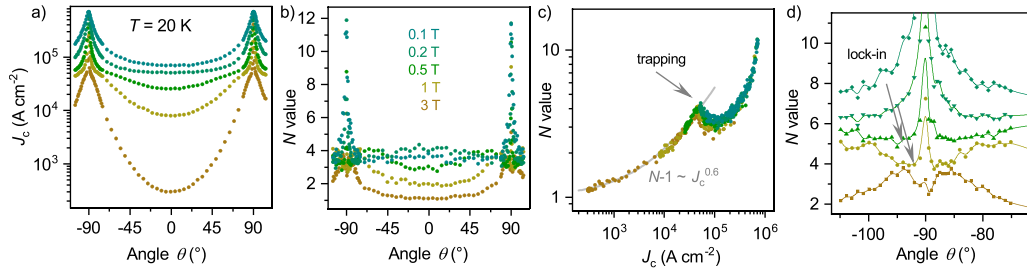


Figure 8. Angular dependence of the critical current density, $J_c(\theta)$, (a) and of the N value (b) at 20 K. Vortex trapping is best seen as anti-correlation in the N vs. J_c scaling (c). (d) zoom-in of the ab -region showing the increase of N in the lock-in region with estimate of the lock-in angle (data shifted by $\Delta N = 1$ consecutively for clarity).

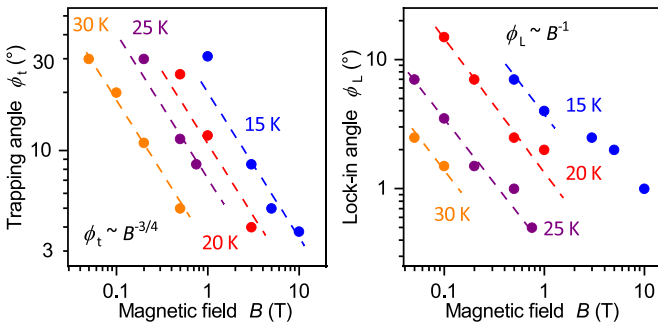


Figure 9. Magnetic field dependence of trapping angle ϕ_t (a) and lock-in angle ϕ_L (b) for several temperatures. The dashed lines are the power law dependencies as given in the panels.

the correct pre-factor in the equation for f_p' as well as slight corrections of ξ and λ due to finite temperature (4 K) and field (1–3 T), the flux lines are individually and very strongly pinned in the field range around 1 T at low temperatures. A maximum pinning force density of $\sim 110 \text{ GN m}^{-3}$ for $B\parallel c$ was measured at 4 K. This is comparable to the best NdFeAs(O,F) films to date [50].

4.2. J_c anisotropy

As can be expected by the large anisotropies in resistivity and critical fields, figure 2, also the critical current density is highly anisotropic, figure 6. At all temperatures and fields, sharp J_c peaks for $B\parallel ab$ ($\theta = \pm 90^\circ$) can be seen whereas for $B\parallel c$ (0°) J_c has a minimum. The general appearance of $J_c(\theta)$ is very similar to $Ln1111$ films, such as LaFeAs(O,F) [31] and NdFeAs(O,F) [50].

The angular dependence of the pinning force, where only small, isotropic, random defects contribute to pinning, is more or less solely determined by the properties of the flux line system, i.e. by intrinsic parameters. That means $J_c(\theta)$ can be scaled with the anisotropic Ginzburg-Landau (AGL) scaling approach to an effective magnetic field $B_{\text{eff}} = B (\cos^2\theta + \gamma^{-2}\sin^2\theta)^{0.5}$ [51], where γ is the anisotropy of B_{c2} for microstructurally sufficiently clean samples with 3D behaviour, as observed e.g. in [31, 52] or rather may follow the λ anisotropy in more 2D-like samples, e.g. [53]. Often nevertheless, $\gamma = \gamma_{\text{eff}}$ is an effective scaling parameter which can e.g. be highly reduced in pinning improved nanocomposites

as often observed for cuprates [54] or lay between the B_{c2} and λ anisotropy in FBS [55].

As can be seen in figure 7, this scaling is possible in a wide angular range around $B\parallel c$ (i.e. at high effective fields), and deviations from this scaling occur near $B\parallel ab$. This is expected due to the layered crystal structure and film geometry. At high temperatures, the critical currents follow $J_c \sim B_{\text{eff}}^{-1}$ (indicated by the black line), which is again a sign for strong pinning at small random pinning centres, see figure 5. At higher fields and especially at lower temperatures, the exponent of the effective-field dependence is again smaller ($J_c \sim B_{\text{eff}}^{-0.5}$), indicating that a further pinning mechanism sets in. At low temperatures and high fields, the scaling approach reveals an asymmetry of the ab -peak (arrows) by the opening of a slight ‘hysteresis’. This can be explained by an inhomogeneity in film thickness, which is hard to avoid in sample fabrication by MHE. A tilted growth as alternative explanation was ruled out by the XRD results. The scaling parameter γ shows some degree of temperature dependence (inset figure 7), although without a clear trend over the entire temperature range. Whereas it seems to extend the B_{c2} anisotropy obtained via resistivity scaling by Wang, Yi *et al* [24, 46] towards lower temperatures, it somewhat levels at higher temperatures. At such high temperatures, the influence of the λ anisotropy (which is close to the ξ anisotropy [23]) cannot be neglected. More realistic models, including two-band superconductivity [56, 57] or the layered crystal structure [58], have not been followed in this study. However, treating the exponent of the scaling function as phenomenological fitting parameter, as successful for BaFe₂As₂ films [59, 60] did not lead to better scaling behaviour in this case.

Highly anisotropic layered superconductors behave as quasi-2D systems at low temperatures and as 3D systems at high temperatures, where the out-of-plane coherence length ξ_c becomes larger than the distance between the superconducting layers d , i.e. in many cases the c -axis parameter. The crossover temperature between these two regimes is given by $T_{\text{cr}} = \left\{ 1 - 2 \frac{\xi_c(0)^2}{d^2} \right\} T_c$ [40]. With $\xi_c(0) = 0.24 \text{ nm}$ and $d = 0.9324 \text{ nm}$, $T_{\text{cr}} \sim 37 \text{ K}$, and thus the sample is in the quasi-2D regime in nearly the entire temperature range, and intrinsic pinning by the layered crystal structure should be expected for field orientations close to the ab -direction. In fact, this had been observed for several FBS films, such

as SmFeAs(O,F) [37, 61], NdFeAs(O,F) [55], and Fe(Se,Te) [53]. This pinning mechanism is not to be confused with pinning at naturally occurring correlated pinning centres in single crystals, which is occasionally also called intrinsic pinning [62, 63].

Pinning at highly correlated structures, such as the crystallographic planes, is characterized by two mechanisms: vortex lock-in and vortex trapping. Vortex lock-in is the pinning of the entire flux line for angles $\phi = \angle(B, ab)$ smaller than the lock-in angle ϕ_L , and vortex trapping means pinning of vortex segments only and concurrent formation of a staircase vortex structure for $\phi_L < \phi < \phi_t$, where ϕ_t is the trapping angle. Both ϕ_t and ϕ_L are temperature and field dependent. One way of distinguishing these two regimes from each other and from pinning by random defects is to evaluate the exponent of the voltage-current characteristics $V(I) \propto I^N$, the N value (i.e. the flux creep exponent), in the vicinity of J_c , as shown exemplarily for the 20 K data in figure 8. For sufficiently homogeneous samples, as for the investigated films, the N value is roughly inversely related to the creep rate $S \sim 1/(N-1)$ of thermally assisted flux creep. For random pinning, both S and J_c depend on the pinning potential U and are, therefore, correlated. Therefore, J_c and N are scaling with positive correlation around B_{llc} where random pinning dominates, figure 8(c). The $N(J_c)$ dependence in this region shows power law behaviour that is ultimately linked to the $V(I)$ scaling around the glass-liquid transition. In the medium J_c range in figure 8(c), an anti-correlation between J_c and N is visible. This is the region of vortex trapping. The vortex segments perpendicular to the ab -planes are pinned much weaker and lead by their easy sideward movement to an effective net movement of the parallel segments. The creep rate S increases, and therefore N decreases. In this region, J_c and N are not positively correlated but show anti-correlation with somewhat less perfect scaling. Instead, $N(\theta)$ for different fields at one temperature scale, since the creep rate S only depends on the number of vortex segments per length of flux line. This effect is shadowed in the present data due to considerable noise; however see also data in references [53, 64]. For medium fields, a narrow peak of $N(\theta)$ is visible within the dip of vortex trapping, figure 8(d). This is the regime of vortex lock-in, where S decreases again because of the absence of weakly pinned vortex segments. At low fields, this effect is smeared out by superposed random pinning; at high fields, a possible lock-in peak is not observed due to the limited angular resolution and the small lock-in angle. As shown in figure 9, the trapping angle follows roughly a $\phi_t \sim B^{-3/4}$ dependence, similar to the observation in [55] on NdFeAs(O,F), and the lock-in angle follows $\phi_L \sim B^{-1}$, which is weaker than theoretically predicted ($\phi_L \sim \phi_t/B$), again as observed in [55].

5. Summary and conclusion

The electrical transport properties of sharply-textured, epitaxial (Li,Fe)OHFeSe films grown by MHE on LaAlO₃ were investigated with focus on the anisotropy. These films with

optimum T_c of ~ 42 K show an anisotropy ratio near T_c of ~ 11 , which is also found in the AGL scaling of the critical current density J_c . The ground-state values of the coherence lengths were estimated via the slopes of B_{c2} (50% criterion) near T_c to be $\xi_{ab} = 2.7$ nm and $\xi_c = 0.24$ nm, in good agreement with a two-band B-WHH model. Due to this short c -axis coherence length, the films are in the 2D superconducting state nearly in the whole superconducting region, and intrinsic flux pinning is observed and characterized by the analysis of the flux creep exponent N . The ground-state value for the penetration depth was estimated via the extrapolation of the self-field $J_c(T)$ dependence in a single-band model for s -, d -, and p -wave order parameter symmetries and was found to be $\lambda_{ab} \sim 160$ – 200 nm, which is considerably smaller than literature values. The field dependence of the activation energy for thermally assisted flux motion U_0 was resolved for low magnetic fields. It agrees well with literature values on corresponding single crystals and follows the expected trend with T_c and electrical anisotropy γ . The field dependencies of U_0 and J_c at low T show both a second region of single vortex pinning at medium fields.

Acknowledgments

The work at China was supported by National Natural Science Foundation of China (Nos.11888101, 11834016), the National Key Research and Development Program of China (Grant Nos. 2017YFA0303003, 2016YFA0300300), and the Strategic Priority Research Program and Key Research Program of Frontier Sciences of the Chinese Academy of Sciences (Grant No. QYZDY-SSW-SLH001, XDB25000000). EFT thanks financial support provided by the state assignment of Minobrnauki of Russia (theme ‘Pressure’ No. AAAA-A18-118020190104-3) and by Act 211 Government of the Russian Federation, contract No. 02.A03.21.0006.

ORCID iDs

Jens Hänisch  <https://orcid.org/0000-0003-2757-236X>
 Dong Li  <https://orcid.org/0000-0002-0823-195X>
 Kui Jin  <https://orcid.org/0000-0003-2208-8501>
 Xiaoli Dong  <https://orcid.org/0000-0002-6268-2049>
 Evgeny Talantsev  <https://orcid.org/0000-0001-8970-7982>
 Bernhard Holzapfel  <https://orcid.org/0000-0002-8420-4777>

References

- [1] Hänisch J, Iida K, Hühne R and Tarantini C 2019 *Supercond. Sci. Technol.* **32** 093001
- [2] Sakoda M, Iida K and Naito M 2018 *Supercond. Sci. Technol.* **31** 093001
- [3] Chang K *et al* 2015 *EPL* **109** 28003
- [4] Huang Y, *et al* Matrix-assisted fabrication and exotic charge mobility of (Li,Fe)OHFeSe superconductor films arXiv:1711.02920
- [5] Lu X F *et al* 2015 *Nat. Mater.* **14** 325

- [6] Pachmayr U, Nitsche F, Luetkens H, Kamusella S, Brückner F, Sarkar R, Klaus H-H and Johrendt D 2015 *Angew. Chem. (Int. Ed. In English)* **54** 293–7
- [7] Sun H *et al* 2015 *Inorg. Chem.* **54** 1958–64
- [8] Dong X, Zhou H, Yang H, Yuan J, Jin K, Zhou F, Yuan D, Wei L, Li J, Wang X, Zhang G, Zhao Z 2015 Phase Diagram of $(\text{Li}_{1-x}\text{Fe}_x)\text{OHFeSe}$: A Bridge between Iron Selenide and Arsenide Superconductors *J. Am. Chem. Soc.* **137** 66–69
- [9] Dong X-L *et al* 2015 *Phys. Rev. B* **92** 064515
- [10] Hsu F, Luo J, Yeh K, Chen T, Huang T, Wu PM, Lee Y, Huang Y, Chu Y, Yan D, Wu M 2008 Superconductivity in the PbO-type structure -FeSe *Proceedings of the National Academy of Sciences* **105** 14262–14264
- [11] Patel U, Hua J, Yu S H, Avci S, Xiao Z L, Claus H, Schlueter J, Vlasko-Vlasov V V, Welp U and Kwok W K 2009 *Appl. Phys. Lett.* **94** 082508
- [12] Wang Q-Y *et al* 2012 *Chin. Phys. Lett.* **29** 037402
- [13] Zhao L *et al* 2016 *Nat. Commun.* **7** 10608
- [14] Huang Y *et al* 2017 *Chin. Phys. Lett.* **34** 077404
- [15] Nelson J B and Riley D P 1945 *Proc. Phys. Soc.* **57** 160–77
- [16] Mao Y *et al* 2018 *Chin. Phys. Lett.* **35** 057402
- [17] Werthamer N R, Helfand E and Hohenberg P C 1966 *Phys. Rev.* **147** 295–302
- [18] Talantsev E F 2019 *Condensed Matter* **4** 83
- [19] Baumgartner T, Eisterer M, Weber H W, Flükiger R, Scheuerlein C and Bottura L 2013 *Supercond. Sci. Technol.* **27** 15005
- [20] Gor'kov L P 1960 *Soviet. Phys. JETP* **10** 593
- [21] Jones C K, Hulm J K and Chandrasekhar B S 1964 *Rev. Mod. Phys.* **36** 74
- [22] Vedenev S I, Piot B A, Maude D K and Sadakov A V 2013 *Phys. Rev. B* **87** 134512
- [23] Khasanov R, Zhou H, Amato A, Guguchia Z, Morenzoni E, Dong X, Zhang G and Zhao Z 2016 *Phys. Rev. B* **93** 224512
- [24] Wang C, Yi X, Qiu Y, Tang Q, Zhang X, Luo Y and Yu B 2016 *Supercond. Sci. Technol.* **29** 055003
- [25] Wang Z-S, Yuan J, Wosnitza J, Zhou H, Huang Y, Jin K, Zhou F, Dong X-L and Zhao Z 2017 *J. Phys.: Condens. Matter* **29** 025701
- [26] Zhang G-Y, Chou M and Lin C-T 2017 *Crystals* **7** 167
- [27] Torres J H S, Ricardo da Silva R, Moehlecke S and Kopelevich Y 2003 *Solid State Commun.* **125** 11–16
- [28] Haindl S *et al* 2010 *Phys. Rev. Lett.* **104** 077001
- [29] Sun Y, Zhang W, Xing Y, Li F, Zhao Y, Xia Z-C, Wang -L-L, Ma X, Xue Q-K and Wang J 2014 *Sci. Rep.* **4** 6040
- [30] Zhao W, Chang C-Z, Xi X, Mak K F and Moodera J S 2016 *2D Mater.* **3** 024006
- [31] Kidszun M, Haindl S, Thersleff T, Hänisch J, Kauffmann A, Iida K, Freudenberger J, Schultz L and Holzapfel B 2011 *Phys. Rev. Lett.* **106** 137001
- [32] Hänisch J, Iida K, Ohmura T, Matsumoto T, Hatano T, Langer M, Kauffmann-Weiss S, Ikuta H and Holzapfel B 2018 *MRS Communications* **8** 1433–8
- [33] Schneider R, Zaitsev A G, Fuchs D and Hott R 2020 *Supercond. Sci. Technol.* **33** 075011
- [34] Ahmad D, Choi W J, Seo Y I, Seo S, Lee S and Kwon Y S 2017 *Results Phys.* **7** 16–20
- [35] Ge J, Cao S, Shen S, Yuan S, Kang B and Zhang J 2010 *Solid State Commun.* **150** 1641–5
- [36] Shahbazi M, Wang X L, Ghorbani S R, Dou S X and Lin C T 2015 *Physica C* **519** 60–64
- [37] Iida K *et al* 2013 *Sci. Rep.* **3** 2139
- [38] Feigel'man M V and Vinokur V M 1990 *Phys. Rev. B* **41** 8986
- [39] Talantsev E F, Iida K, Ohmura T, Matsumoto T, Crump W P, Strickland N M, Wimbush S C and Ikuta H 2019 *Sci. Rep.* **9** 14245
- [40] Blatter G, Feigel'man M V, Geshkenbein V B, Larkin A I and Vinokur V M 1994 *Rev. Mod. Phys.* **66** 1125–388
- [41] Lao M *et al* 2019 *Supercond. Sci. Technol.* **32** 94003
- [42] Talantsev E F and Tallon J L 2015 *Nat. Commun.* **6** 7820
- [43] Khasanov R, Shengelaya A, Maisuradze A, Di Castro D, Savić I M, Weyeneth S, Park M S, Jang D J, Lee S-I and Keller H 2008 *Phys. Rev. B* **77** 184512
- [44] Shengelaya A, Khasanov R, Eshchenko D G, Di Castro D, Savić I M, Park M S, Kim K H, Lee S-I, Müller K A and Keller H 2005 *Phys. Rev. Lett.* **94** 127001
- [45] Schneider T 2007 *EPL* **79** 57005
- [46] Yi X, Wang C, Tang Q, Peng T, Qiu Y, Xu J, Sun H, Luo Y and Yu B 2016 *Supercond. Sci. Technol.* **29** 105015
- [47] Iida K, Hänisch J and Tarantini C 2018 *Appl. Phys. Rev.* **5** 031304
- [48] Yamasaki H 2016 *Supercond. Sci. Technol.* **29** 065005
- [49] Matsushita T 2014 *Flux Pinning in Superconductors (Springer Series in Solid-State Sciences)* Vol. 178 (Berlin: Springer) pp 214
- [50] Kauffmann-Weiss S *et al* 2019 *Nanoscale Adv.* **1** 3036–48
- [51] Blatter G, Geshkenbein V B and Larkin D J 1992 *Phys. Rev. Lett.* **68** 875–8
- [52] Hänisch J, Iida K, Haindl S, Kurth F, Kauffmann A, Kidszun M, Thersleff T, Freudenberger J, Schultz L and Holzapfel B 2011 *IEEE Trans. Appl. Supercond.* **21** 2887–90
- [53] Iida K *et al* 2013 *Phys. Rev. B* **87** 104510
- [54] Gutiérrez J *et al* 2007 *Nat. Mater.* **6** 367–73
- [55] Tarantini C *et al* 2016 *Sci. Rep.* **6** 36047
- [56] Askerzade I N and Güzel M S 2019 *J Supercond. Nov. Magn.* **32** 1921–6
- [57] Li Y, Kang G and Gao Y 2016 *Physica B* **491** 70–78
- [58] Fastampa R, Sarti S, Silva E and Milani E 1994 *Phys. Rev. B* **49** 15959
- [59] Hänisch J *et al* 2015 *Sci. Rep.* **5** 17363
- [60] Iida K, Sato H, Tarantini C, Hänisch J, Jaroszynski J, Hiramatsu H, Holzapfel B and Hosono H 2017 *Sci. Rep.* **7** 39951
- [61] Iida K, Hänisch J and Naito M 2017 *Teion Kogaku J. Cryo. Super. Soc. Jpn.* **52** 443–7
- [62] Prozorov R, Tanatar M A, Ni N, Kreyssig A, Nandi S, Bud'ko S L, Goldman A I and Canfield P C 2009 *Phys. Rev. B* **80** 174517
- [63] Amigó M L, Crivillero M V A, Franco D G, Badía-Majós A, Guimpel J, Campo J, Damay F, Porcher F, Condó A M and Nieva G 2017 *Supercond. Sci. Technol.* **30** 085010
- [64] Civale L, Maiorov B, MacManus-Driscoll J L, Wang H, Holesinger T G, Foltyn S R, Serquis A and Arendt P N 2005 *IEEE Trans. Appl. Supercond.* **15** 2808–11